Hindawi
International Journal of Optics
Volume 2023, Article ID 8017726, 13 pages
https://doi.org/10.1155/2023/8017726

Research Article

Research on the Seed Respiration CO_2 Detection System Based on TDLAS Technology

Lu Gao,[1] **Ying Zang**,[1] **Guangwu Zhao**,[2] **Hengnian Qi**,[1] **Qizhe Tang**,[1] **Qingshan Liu**,[1] **and Liangquan Jia**[1,3]

[1]*School of Information Engineering, Huzhou University, Huzhou 313000, China*
[2]*College of Advanced Agricultural Sciences, Zhejiang A & F University, Hangzhou 311300, China*
[3]*College of Biosystems Engineering and Food Science, Zhejiang University, Hangzhou 310058, China*

Correspondence should be addressed to Ying Zang; 02750@zjhu.edu.cn and Liangquan Jia; 02426@zjhu.edu.cn

Received 21 June 2022; Revised 20 January 2023; Accepted 4 March 2023; Published 22 March 2023

Academic Editor: Yuan-Fong Chou Chau

The traditional detection method of CO_2 concentration in seed respiration has defects such as low detection accuracy, low detection efficiency, and inability to monitor in real time. In order to solve these problems, we report a seed respiration CO_2 detection system based on wavelength modulation spectroscopy (WMS) techniques in tunable diode laser absorption spectroscopy (TDLAS). This system uses a 2004 nm distributed feedback (DFB) laser as the light source, and a double-layer seed respiration device (about 1.5 L) is designed based on Herriott cell with an effective optical path of about 21 meters. Then, the second harmonic ($2f$) signal is extracted by the wavelength modulation method for CO_2 concentration inversion. When the ambient temperature and pressure changes greatly, the corrected $2f$ signal is used for CO_2 concentration inversion to improve the accuracy. A series of verification and comparison experiments have proved that the seed respiration CO_2 detection system has the advantages of strong stability, high sampling frequency, and high detection accuracy. Finally, we used the developed system to measure the respiration intensity and respiration rate of 1 g corn seeds. The respiration intensity curves and respiration rate change details show that the seed respiration CO_2 detection system is more suitable for a small amount of seeds than nondispersive infrared (NDIR) CO_2 sensor and gas chromatography in real-time monitoring of the breathing process.

1. Introduction

Respiration is an important physiological phenomenon of seeds. There is a big difference in nature and respiration strength between distinct seeds. Seeds produce CO_2 and consume O_2 in the process of aerobic respiration. The intensity of seeds aerobic respiration reflects the seed vitality [1–3] and the strength of seed metabolism. Therefore, the study of seed respiration is of great significance to understand the physiological and biochemical processes of seed vigor, seed metabolism, and seed germination.

Common methods for detecting seed respiration include the small basket method, Warburg microrespirometer, Q2 oxygen sensor technology, gas chromatography, and NDIR CO_2 sensor. The small basket method [4] is also called the titration method with the advantage of simple operation. However, the small basket method will cause damage to the seeds and has large human operating errors and low accuracy. Thus, it is not suitable for studying the process of seed respiration with the small basket method. The Warburg microrespirometer [5] can improve the sensitivity and accuracy of seed respiration detection to a certain extent, but it is only applicable to the respiration detection of batches seeds. Due to its special breathing chamber structure, constant temperature is required during the experiment. The Q2 oxygen sensor technology [6, 7] can measure the oxygen consumption data of a single seed during the germination process and analyze the characteristics of the oxygen consumption curves comprehensively. But the sampling interval of seed respiration oxygen consumption data is about 30 minutes to 1 hour, so the time resolution is low and the measurement period generally takes more than 2 days. What is more, only the respiratory intensity

of seed germination stage can be measured using Q2 oxygen sensor technology, for the confined space will have a coercion on seed respiration with time increasing. Gas chromatography is mostly used to measure high molecular weight gas, and it also has high measurement accuracy for CO_2, but its detection process is more complicated. The studied gas needs to be collected and filled into the gas chromatography, making it difficult to monitor seed respiration continuously. Besides, we can only get the gas volume fraction not the gas concentration directly. Therefore, there are still certain limitations in the application of seed respiration detection for using gas chromatography. The above detection methods are all nonspectral analysis methods, and the measurement principle is relatively simple, but the biggest difficulty is that the sampling process is complicated and not real time. Using the NDIR CO_2 sensor to measure seed respiration has fast response time and low detection cost, which shortens the seed respiration detection cycle to a certain extent. But unfortunately, the accuracy of NDIR CO_2 sensors is generally 30–50 ppm, and seed respiration detection devices need to be designed again and again according to different types of NDIR CO_2 sensors [8, 9]. In summary, most traditional seed respiration detection methods require long-term collection of CO_2 emitted by the test samples. The workload of detection and analysis is large, and most of them are destructive testing.

TDLAS has the characteristics of high sensitivity and high resolution and has been widely used in trace gas detection [10–14]. Many scholars at home and abroad have conducted research on TDLAS technology in the CO_2 concentration detection method and detection sensitivity [15–19]. TDLAS detection methods mainly include WMS and direct absorption spectroscopy. WMS can eliminate the low-frequency noise interference caused by the laser itself and the temperature and current during detection. Compared with direct absorption spectroscopy technology, WMS is easier to extract rich harmonic information and obtain a higher signal-to-noise ratio of the detection system, and the gas detection limit is easier to reach ppm or even ppb level [20, 21]. Based on the quadrature demodulation method, the use of the first harmonic to normalize the second harmonic ($2f/1f$) for gas concentration inversion can eliminate the dependence of laser power [22].

Aiming at the problems of seed respiration CO_2 detection, combined with the development of TDLAS in CO_2 detection technology, we have developed a high-sensitivity seed respiration CO_2 detection system based on WMS-TDLAS. Then, we compared the performance of our developed system with the NDIR CO_2 sensor and gas chromatography. A corn seeds respiration test was carried out in a laboratory environment. The test results show that the seed respiration CO_2 detection system has reached the design expectations. The main contributions or innovation of this article are as follows:

(1) Based on Herriot cell, a 21 m effective optical path double-layer seed respiration detection device is designed for the first time, and a seed respiration CO_2 detection system is built based on WMS-TDLAS technology. The cost is relatively low, and real-time online detection can be realized, which solves the situation of no special seed respiration CO_2 detection sensor at present.

(2) The sampling frequency of the seed respiration CO_2 detection system was 7 Hz and the detection limit was 1.23 ppm, and the respiratory changes of a small number of seeds could be detected. The linearity and stability of our developed system is good, and the CO_2 concentration of seed respiration online monitoring with high precision and high time resolution is achieved. Compared with gas chromatography or NDIR CO_2 sensor, its time resolution is tens to hundreds of times higher. Therefore, the seed respiration CO_2 detection system can effectively observe the changes of seed respiration and provide an accurate respiration detection sensor for the in-depth study of seed physiological changes.

(3) A correction method for temperature and pressure is proposed with the second harmonic for concentration inversion. The correction relationship between temperature or pressure changes and $2f$ peak value is calculated, which provides a theoretical method and correction equation for accurate inversion of seed respiration CO_2 concentration in different environments. Thus, the sensor can work in a wide range of temperature and pressure, which expands the application scenario of seed respiration detection.

2. Materials and Methods

2.1. Theoretical Principle. A monochromatic light beam passing through a uniform gas medium will lose intensity due to optical absorption by gas molecules. This process can be described by Beer–Lambert law [23, 24]:

$$\begin{aligned} I_t &= I_0 \exp\left[-PS(T)CL\phi(\nu)\right] = I_0 \exp\left[-\alpha(\nu)L\right] \\ \alpha(\nu) &= \sigma(\nu)\cdot C, \end{aligned} \tag{1}$$

where I_0 is the intensity of laser without CO_2 absorption, P is the total gas pressure (atm), $S(T)$ is the absorption line intensity as a function of temperature, C is the concentration of CO_2 produced by the respiration of tested seeds, L is the effectiveness of the absorption cell optical path (cm), $\varphi(\nu)$ is the absorption linear function of gas molecules, $\alpha(\nu)$ is the absorption rate function, and $\sigma(\nu)$ is the absorption cross section.

TDLAS technology measurement methods include direct absorption spectroscopy and WMS. Among them, direct absorption spectroscopy [25, 26] uses the change of laser intensity after gas absorption to analyze the concentration of the measured gas. Due to the low concentration of CO_2 produced by seed respiration, the gas absorbs less incident laser intensity. Therefore, the fluctuation of laser intensity, the density change of the gas to be measured, and the selection of the baseline will all cause large measurement errors in direct absorption spectroscopy. In order to solve the accurate online measurement of the CO_2 concentration of seed respiration in harsh environments, we use the WMS algorithm [27, 28] to improve the detection accuracy and sensitivity of the TDLAS technology.

Inject a high-frequency sine wave into the laser for high-frequency modulation; the instantaneous frequency $v(t)$ of the laser can be described as

$$v(t) = v0 + \delta v \cos(2\pi f t), \tag{2}$$

where v_0 is the laser center frequency, δv is the modulation amplitude, and f is the sine wave frequency. Then, the cosine expansion of the laser intensity I_t after gas absorption is carried out by Fourier series:

$$I_t(v0, t) = \sum_{n=0}^{\infty} An(v0)\cos(n2\pi f t). \tag{3}$$

Design two reference signals with a phase difference of 90° and use the phase sensitive detection (PSD) algorithm to obtain the n-th harmonic signal component An of the absorption spectrum signal as

$$An(v0) = \frac{2}{\pi}\int_0^{\pi} I0(v0 + \delta v \cos 2\pi f t)\exp\left[-\sigma(v0 + \delta v \cos 2\pi f t)CL\right]\cos(n2\pi f t)d(2\pi f t). \tag{4}$$

Ideally, $I0$ has nothing to do with $v(t)$, so there is no amplitude modulation, and $I0$ is a constant. Thus, equation (4) can be rewritten as

$$An(v0) = \frac{2I0}{\pi}\int_0^{\pi} \exp\left[-\sigma(v0 + \delta v \cos 2\pi f t)CL\right]\cos(n2\pi f t)d(2\pi f t). \tag{5}$$

In general, when the absorption rate function $\alpha(v)L \ll 1$,

$$An(v0) = \frac{2I0CL}{\pi}\int_0^{\pi} -\sigma(v0 + \delta v \cos 2\pi f t)\cos(n2\pi f t)d(2\pi f t). \tag{6}$$

Expanding the formula (6) according to Taylor series, we can get An as follows:

$$An(v0) = \frac{2^{1-n}I0CL}{n!}\sigma^n \frac{d^n\sigma(v)}{dv^n}\bigg|_{v=v0}. \tag{7}$$

As shown in formula (7), the n-th harmonic amplitude of CO_2 absorption signal of seed respiration is proportional to the gas concentration. Since the absorption spectrum of CO_2 is symmetrical about the center frequency, the odd harmonics of the absorbed energy are zero and the even harmonics reach the maximum at $v0$. For even harmonics of different orders, the value at $v0$ decreases as the order increases and the amplitude of the $2f$ signal is the largest. Therefore, considering the symmetry and amplitude of the harmonics and avoiding the influence of the phase error, we use the amplitude of the second harmonic to perform concentration inversion and calculate the CO_2 concentration produced by seed respiration.

2.2. Selection of Spectral Absorption Lines. The seed respiration CO_2 detection system based on WMS-TDLAS technology is mainly used to monitor the concentration of seed respiration CO_2 in real time. By analyzing seed respiration intensity and respiration rate, seed vigor can be determined quickly, nondestructively, and efficiently. Therefore, CO_2 is the target gas. In order to measure the concentration of CO_2 in seed respiration accurately, it is necessary to perform spectral simulation to determine whether the selected line has sufficient absorption line strength and can avoid interference from other gases. In the detection of seed respiration intensity, the main interference gas is H_2O. Both CO_2 and H_2O have absorption bands around 1.6 μm and 2.0 μm [29]. The absorption line of CO_2 near 2.0 μm is stronger than that near 1.6 μm, and the absorption of H_2O near 2.0 μm is weaker.

In an environment of 1 atm, room temperature, and a light path of 21 meters, based on the HITRAN 2016 database, the 2000 nm band is used to perform absorption simulation calculations for 400 ppm CO_2 and 1% H_2O [30]. The simulated absorbance of CO_2 is shown in Figure 1(a). It can be seen that there are several CO_2 absorption lines near the 2004 nm band and H_2O has little interference with CO_2 in this band. There are three strong absorption lines near the frequency of 4989 cm^{-1}–4993 cm^{-1}, with the center frequencies of 4990 cm^{-1}, 4991.25 cm^{-1}, and 4992.5 cm^{-1}, respectively. Considering the cost-effectiveness of the laser, we choose the 2004 nm DFB laser (nanoplus, maximum power 5 mW, Germany) for seed respiration intensity detection.

When the effective optical length, temperature, and pressure are determined, the driving current will affect the center frequency of the absorption spectrum. Figure 1(b) shows the absorption spectrum of CO_2 under different driving currents

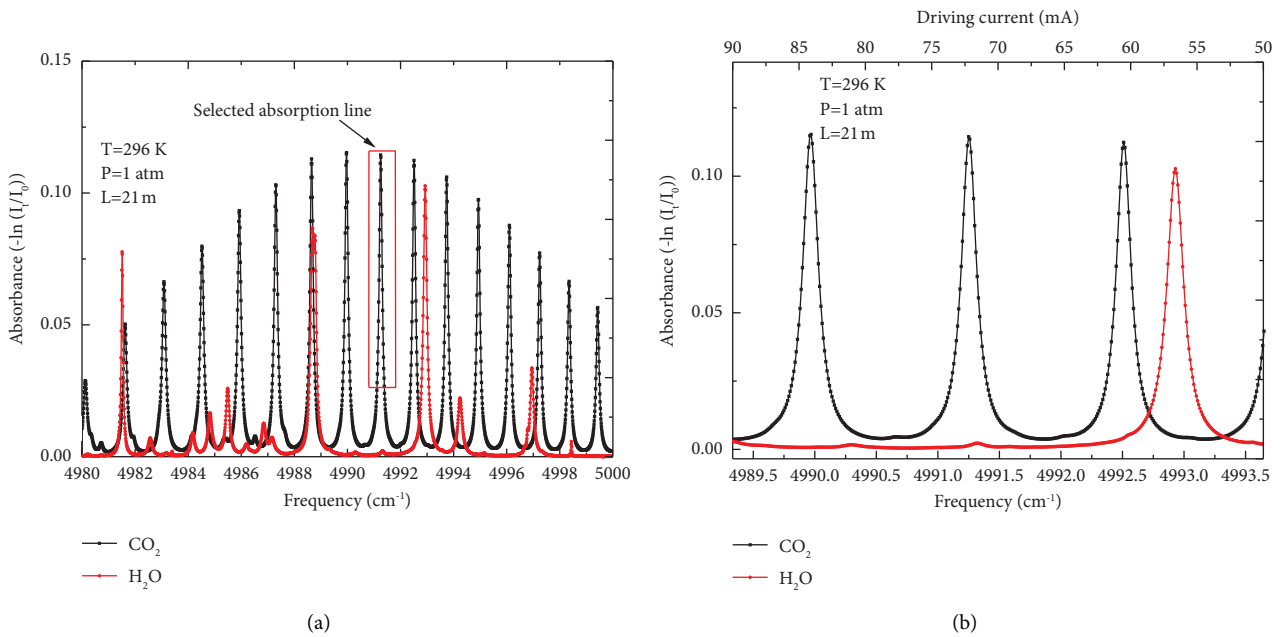

FIGURE 1: Absorption simulation calculations for 400 ppm CO_2 and 1% H_2O. (a) Simulation of spectral absorption of 400 ppm CO_2 and 1% H_2O at pressure of 1 atm, with the near wavelength regions 2000 nm, path length 21 m; (b) simulation of spectral absorption with 400 ppm CO_2 and 1% H_2O in different driving current (50 mA–90 mA).

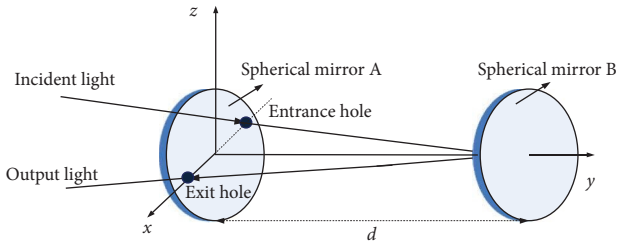

FIGURE 2: Herriott pool reflection model.

(50 mA–90 mA). In order to select the CO_2 absorption line with a center frequency of 4991.25 cm^{-1} accurately, we set the DFB laser driving current to 70 mA.

2.3. Experimental Systems. Our developed double-layer seed respiration device includes seed respiration chamber and Herriott cell. A rectangular cover is arranged above the seed respiration chamber, and a silicone ring is used to seal between the rectangular cover and the seed respiration chamber. When the silicone ring is squeezed and deformed by the pressure from the cover, the double-layer seed respiration device is sealed to avoid the influence of external air in the seed respiration detection. A filter screen is set between the seed respiration chamber and the Herriott cell with a steel mesh structure; thus, the gas between the seed respiration chamber and the Herriott cell is fully diffused, while impurities and dust in the seeds are prevented from falling into the Herriott cell. The respiration space of seeds is relatively large, so there is no need to consider the inhibition of seed respiration by changes in concentration of CO_2 and O_2.

The Herriott cell is composed of two spherical mirrors A and B placed on opposite sides, with a schematic diagram of the basic structure shown in Figure 2.

The laser emits from the entrance hole and then exits from the exit hole after multiple reflections, forming a complete reflection light path. The light path transmission matrix is shown as

$$\cos(K\pi/N) = \sqrt{g_1 g_2}, \tag{8}$$

where N is the number of reflected light spots on one of the spherical mirrors, K is the number of times the light ray rotates around the optical axis, and $K < N$, N is not divisible by K. We define $g_1 = 1 - (d/R_1)$, $g_2 = 1 - (d/R_2)$, where d is the distance between the two spherical mirrors, R_1 and R_2 are the radii of curvature of spherical mirrors A and B. Generally, $R_1 = R_2 = R$, and d can be calculated as

$$d = R(1 - \cos\theta), \tag{9}$$

where $\theta = (K\pi/N)$, $0 < \theta < \pi$.

A relatively large effective optical path can be obtained by increasing the number of reflections. When a light spot is close to the exit hole with a large radius, part of the laser may leak from the Herriott cell and reach the detector during the reflection process. At this time, there will be a large error between the measured optical path and the target optical path. Therefore, the size of the entrance hole and the exit hole should be as small as possible. In addition, the distribution of light spots should be close to the edge of the spherical mirrors to accommodate more light spots. Due to the influence of reflectivity of spherical mirrors, too many reflections means more light intensity attenuation, which will reduce the signal-to-noise ratio and affect the stability of the optical path. Based on the above research and development concept, we use the TracePro software (V8.1, LAMBDA research corporation,

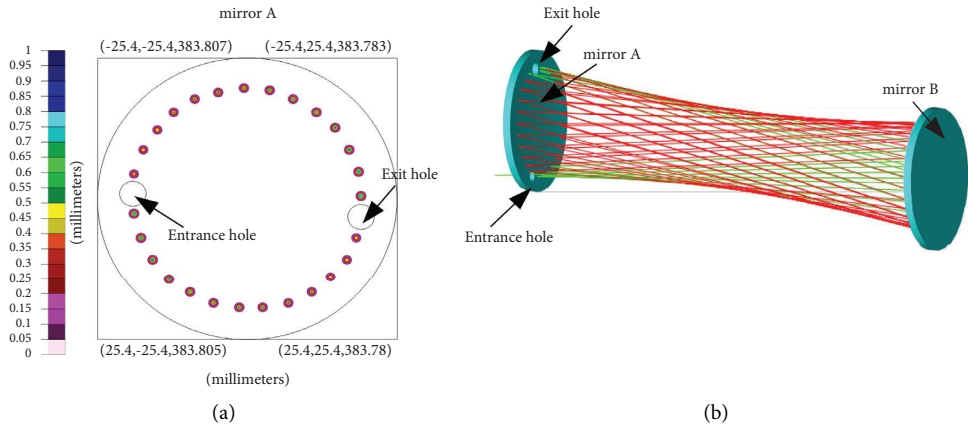

(a) (b)

Figure 3: Optical path simulation of Herriott cell. (a) Light spots simulation of Herriott cell, totally 27 light spots on mirror *A* (there are 28 light spots on mirror *B*); (b) reflected light path simulation of Herriott cell between two spherical mirrors with a diameter of 2 inches and a radius of curvature of 400 mm and a center distance of 378.4 mm.

USA) to simulate and design the reflected light path of Herriott cell. Considering the influence of factors such as processing cost and system detection accuracy, the two spherical mirrors are set with a diameter of 2 inches and a radius of curvature of 400 mm and a center distance of 378.4 mm. Two off-axis holes with a diameter of 4 mm are opened partly at a distance of 20 mm from the center of the spherical mirror A as the entrance and exit holes of the laser. The reflected light path and light spot distribution diagram are shown in Figure 3.

28 light spots are formed on the spherical mirror *B*, and the total optical path is about 20.41 m. With the increase in the number of reflections, the size of the light spots does not increase, indicating that the Herriott cell has a better focusing ability for the light path. The two spherical mirrors are connected by a cylinder in the middle, and the lenses are coated with a mid-infrared high-reflection film. The entrance and exit laser adopts an adjustable structure, equipped with FC/APC standard connectors (F028APC-2000, THORLABS). Based on the above simulation results, we developed a double-layer seed respiration device with a volume of about 1.5 L, which has the advantages of long optical path, relatively small volume, wide temperature adaptation range, strong focusing ability, corrosion resistance, and easy installation and operation. The double-layer seed respiration device is shown in Figure 4.

The seed respiration CO_2 detection system is shown in Figure 5, which mainly includes a double-layer seed respiration device for placing seeds (one to hundreds of seeds can be placed), a circuit and control module, and a data processing module. The DFB laser is driven by a temperature current controller, and the scanning frequency of the driver is 50 Hz. The laser is focused by the collimator into the Herriott cell of the double-layer seed respiration device to detect the CO_2 concentration. The laser is received by the detector after multiple reflections in the Herriott cell, and then after two-stage amplification, the signal is collected and recorded by the DAQ data acquisition card. Then, the upper computer software performs spectral signal filtering, 2*f* signal demodulation, and inversion of gas concentration.

When the temperature changes, the temperature drift of the circuit components will aggravate the varieties in the working conditions of the DFB laser. Therefore, it is necessary to control the temperature of the DFB laser accurately and perform the temperature compensation. In addition, in order to obtain the stable wavelength of the DFB laser, we designed a wavelength closed-loop locking method. After the spectrum signal is collected by the upper computer software, the absorption peak position is calculated. The direction of wavelength drift is determined according to the error between the current absorption peak position and the target absorption peak position. And then, a wavelength adjust signal is sent to the MCU (STM32H743VIT6) to adjust the output wavelength of the DFB laser.

3. Results and Discussion

3.1. Signal Processing. In order to obtain the measurement data of the project quickly and accurately, we prefer to filter and smooth the obtained seed respiratory CO_2 spectral signal by using Savitzky Golay based on empirical mode decomposition (EMD-SG) filtering algorithm [31, 32] after cumulative average and normalization. EMD-SG filtering algorithm can fully retain the useful information in the spectral signal and improve the signal-to-noise ratio. Then, the PSD algorithm is used to extract the 2*f* signal from the denoised seed respiratory CO_2 spectral signal. Finally, the ratio of the peak value of the 2*f* signal to the peak value of the calibrated gas 2*f* signal is used to calculate the CO_2 concentration of seed respiration. The detail step of the specific data acquisition process is presented as follows and is shown in Figure 6:

(1) Obtain the effective seed respiration CO_2 absorbance spectrum signal and filtering

We use the EMD-SG algorithm for denoising and filtering shown in Figure 7. The CO_2 absorbance spectrum is decomposed by EMD to get IMF and residual component. The previous few IMF have the most significant *C* and residual component to get the denoising reconstructing signal. After that, the denoising reconstructing signal is smoothed by SG filter based on improving particle swarm

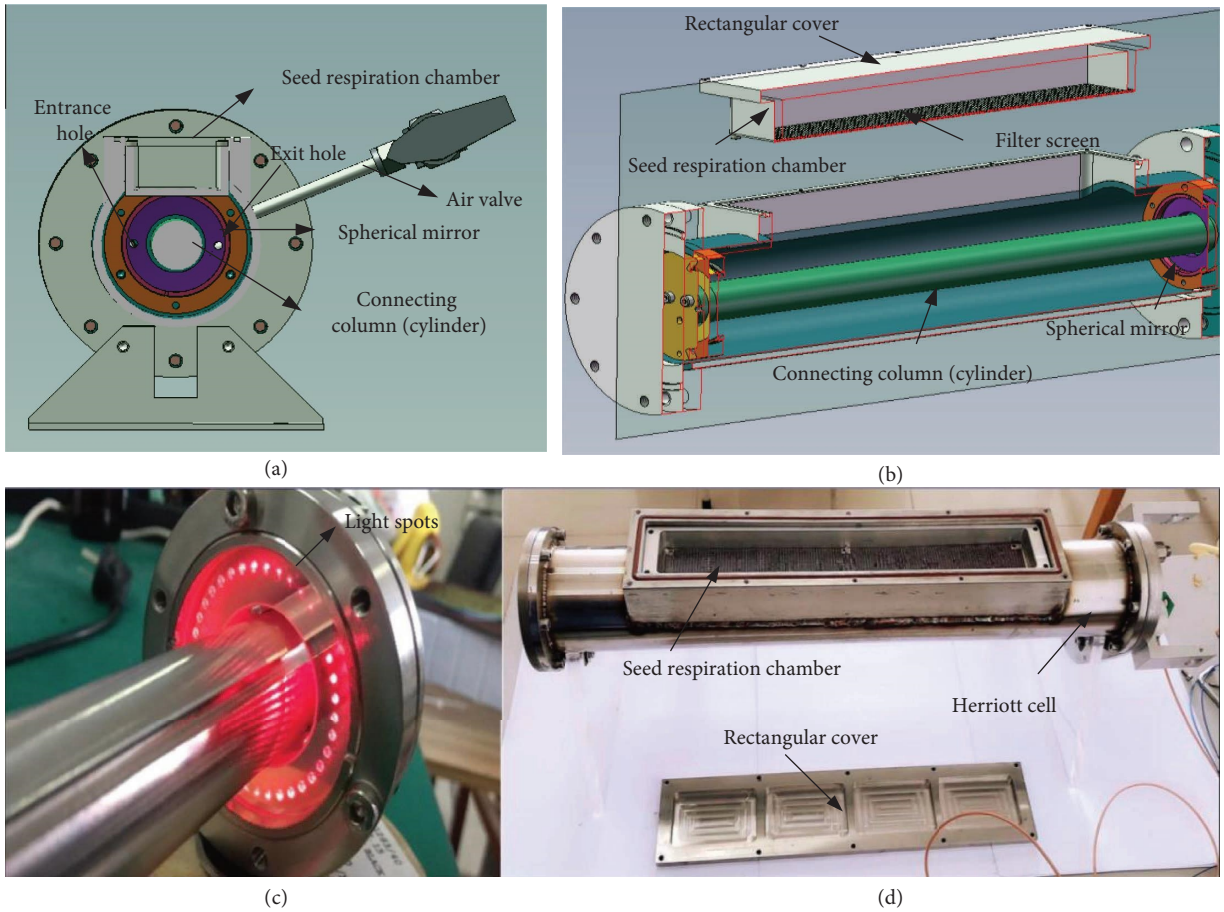

Figure 4: The double-layer seed respiration device. (a) XY plane sectional view of the double-layer seed respiration device; (b) YZ plane sectional view of the double-layer seed respiration device; (c) light spots of the spherical mirror; (d) physical diagram of the double-layer seed respiration device.

optimization (PSO) algorithm with an appropriate window size and polynomial order.

(2) Extract $2f$ signal with PSD algorithm and its parameters setting

The most important thing in the demodulation of $2f$ signal is to set the parameters reasonably to enhance the signal-to-noise ratio and obtain a high-quality second harmonic lineshape. In order to avoid the influence of the phase error, the PSD algorithm is used to extract the $2f$ signal from the denoised effective seed respiration CO_2 absorption spectrum. The phase difference between two reference signals of the PSD algorithm is 90°, which ensures that the quadrature output result remains constant with the initial phase changing. The denoised effective seed respiration CO_2 absorption spectrum $X(t)$ is expressed as Fourier series:

$$X(t) = V_{s1}\sin(\omega_0 t + \varphi_1) + V_{s2}\sin(2\omega_0 t + \varphi_2) + V_{s3}\sin(3\omega_0 t + \varphi_3) + \cdots + n(t). \tag{10}$$

And the reference signal is set as

$$R(t) = V_r \sin(\omega_r t + \theta). \tag{11}$$

We multiply effective seed respiration CO_2 absorption spectrum $X(t)$ and the reference signal $R(t)$ to get $V_{out}(t)$:

$$\begin{aligned} V_{out}(t) = {} & V_r V_{s1}\sin(\omega_r t + \theta)\sin(\omega_0 t + \varphi_1) + V_r V_{s2}\sin(\omega_r t + \theta)\sin(2\omega_0 t + \varphi_2) \\ & + V_r V_{s3}\sin(\omega_r t + \theta)\sin(3\omega_0 t + \varphi_3) + \cdots + V_r \sin(\omega_r t + \theta) n(t). \end{aligned} \tag{12}$$

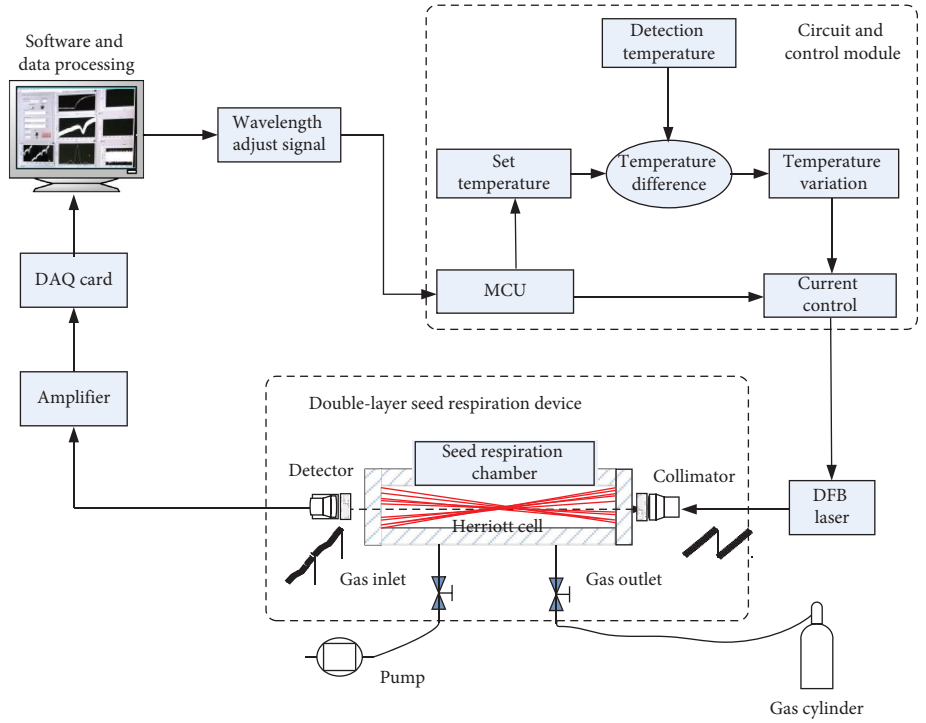

Figure 5: Schematic of the seed respiration CO_2 detection system based on WMS-TDLAS.

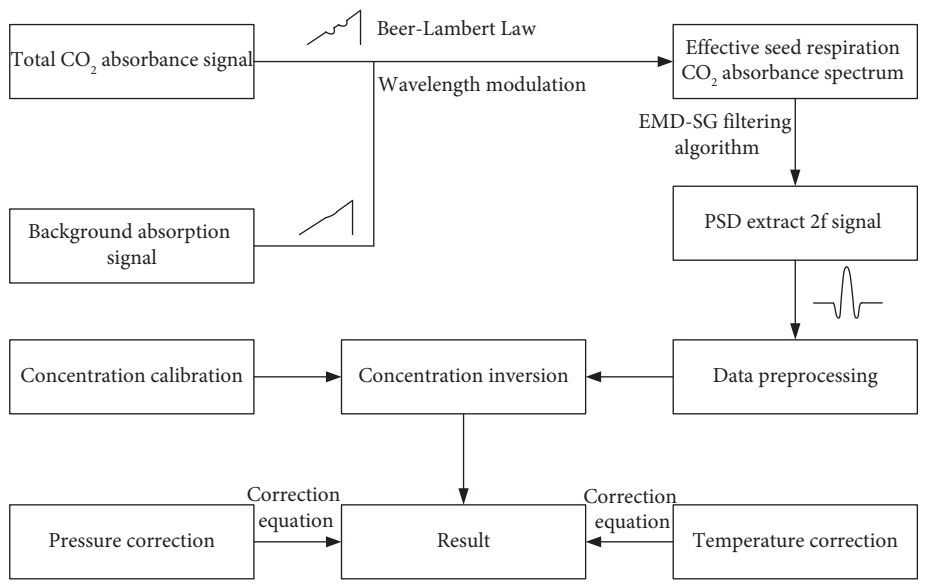

Figure 6: Flowchart of spectral data processing and correction.

The trigonometric function formula is used to expand $V_{\text{out}}(t)$:

$$\begin{aligned} V_{out}(t) = {} & 0.5V_rV_{s1}\cos\left[(\omega_0-\omega_r)t+(\varphi_1-\theta)\right]-0.5V_rV_{s1}\cos\left[(\omega_0+\omega_r)t+(\varphi_1+\theta)\right] \\ & +0.5V_rV_{s2}\cos\left[(2\omega_0-\omega_r)t+(\varphi_2-\theta)\right]-0.5V_rV_{s2}\cos\left[(2\omega_0+\omega_r)t+(\varphi_2+\theta)\right] \\ & +0.5V_rV_{s3}\cos\left[(3\omega_0-\omega_r)t+(\varphi_3-\theta)\right]-0.5V_rV_{s3}\cos\left[(3\omega_0+\omega_r)t+(\varphi_3+\theta)\right]+ \\ & \cdots+V_rn(t)\sin\left(\omega_rt+\theta\right). \end{aligned} \tag{13}$$

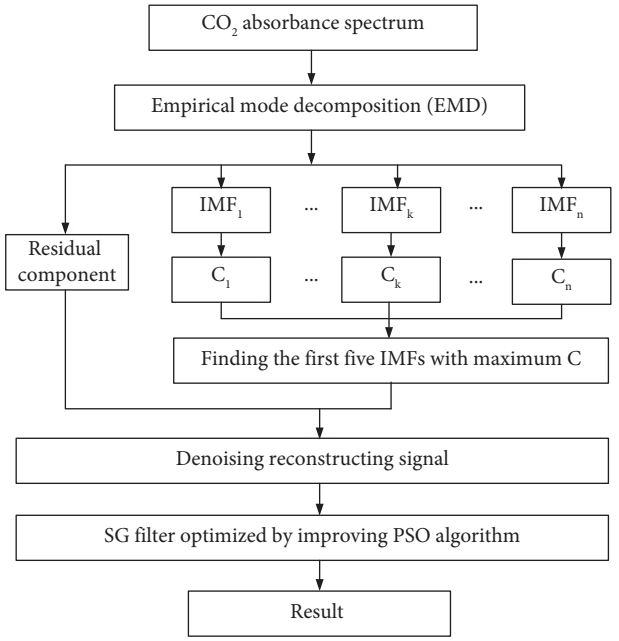

Figure 7: Flowchart of EMD-SG algorithm for denoising and filtering of CO_2 absorbance spectrum signal.

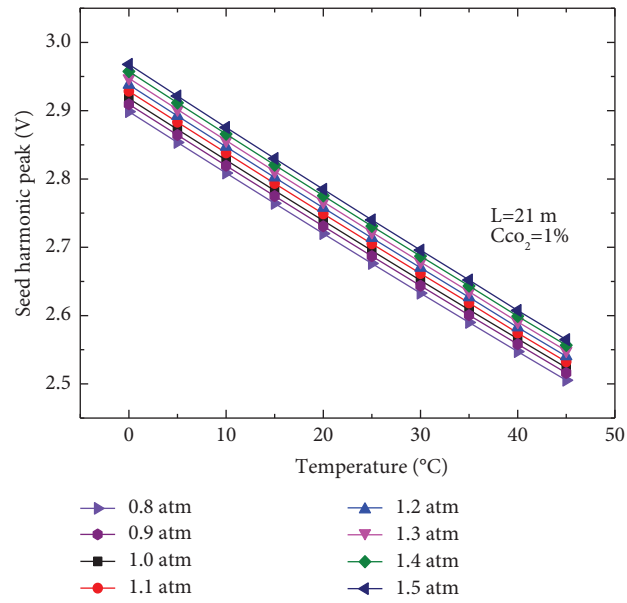

Figure 8: Correction of second harmonic peak with 1% CO_2 at different temperature (0°C–45°C), path length 21 m.

In order to extract the $2f$ signal, we set the parameter as $\omega_r = 2\omega_0$; then, $V_{\text{out}}(t)$ is

$$\begin{aligned} V_{out}(t) &= 0.5V_rV_{s1}\cos\left[\omega_0 t + (\varphi_1 - \theta)\right] - 0.5V_rV_{s1}\cos\left[3\omega_0 t + (\varphi_1 + \theta)\right] \\ &+ 0.5V_rV_{s2}\cos(\varphi_2 - \theta) - 0.5V_rV_{s2}\cos\left[(4\omega_0)t + (\varphi_2 + \theta)\right] \\ &+ 0.5V_rV_{s3}\cos\left[\omega_0 t + (\varphi_3 - \theta)\right] - 0.5V_rV_{s3}\cos\left[(5\omega_0)t + (\varphi_3 + \theta)\right] + \\ &\cdots + V_r n(t)\sin(2\omega_0 t + \theta). \end{aligned} \tag{14}$$

In addition to the DC signal, the output signal $V_{out}(t)$ also contains 1st order harmonic frequency, 2nd order harmonic frequency, and high order harmonic frequency components. Low-pass filtering is used to retain the DC signal $0.5V_rV_{s2}\cos(\varphi_2 - \theta)$ from $V_{out}(t)$. It is necessary to set the low-pass filter cutoff frequency $\omega_s < \omega_0$, and the pass-band cut-off frequency ω_p should be greater than the scanning signal frequency. In this project, the signal scanning frequency is set as 50 Hz and the modulation frequency is set as 200 KHz. We use the Butterworth filter to filter the signal with its parameters of $\omega_p = 2 \times 10^{-5}$ rad/s, $\omega_s = 0.064$rad/s, the maximum attenuation of the pass band $Rp = 1$ dB, and the minimum attenuation of the stop band $Rs = 55$ dB.

(3) Correction of $2f$ signal in different temperature and pressure

In the process of concentration inversion, if temperature and pressure vary widely, they need to be corrected. The seed respiration CO_2 detection system developed in this study is operated under standard atmospheric pressure or a gas environment of the same pressure during the test process, so the pressure change can be ignored in the measurement process. However, the temperature varies greatly when the user measures at different times in different weather, so it is necessary to correct the measurement results of seed respiration at different temperatures. Under the same modulation factor, the second harmonic peak value will decrease as the temperature increases. Figure 8 shows the relationship between the peak value of the second harmonic and the temperature under the environment of 21 m effective optical path, 0°C–45°C, 0.8°atm–1.5 atm.

At 1 atm, the third-order polynomial is used to analyze CO_2 with a volume fraction of 1%. The peak change of the $2f$ signal of gas is fitted, and the fitting equation is obtained as

$$Y = B_3T_0^3 + B_2T_0^2 + B_1T_0 + B_0, \tag{15}$$

where $B_0 = 2.9246$, $B_1 = -0.0089$, $B_2 = -5.199 \times 10^{-6}$, $B_3 = 3.637 \times 10^{-8}$, and T is the temperature at any moment. The peak values of the $2f$ signal at different temperatures are corrected to the test situation of the reference temperature

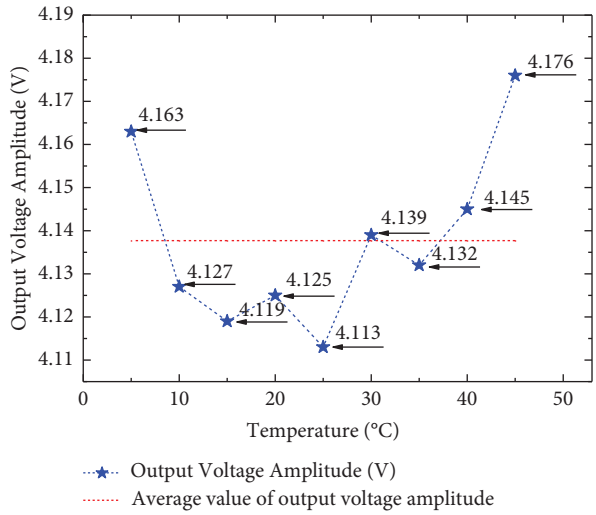

Figure 9: Stability test of laser output.

T_0 ($T_0 = 20^\circ$C). The corrected second harmonic peak F_T is shown in formula (15), and similar methods can be used for correction under other pressure conditions.

$$F_T = \frac{B_3T_0^3 + B_2T_0^2 + B_1T_0 + B_0}{B_3T^3 + B_2T^2 + B_1T + B_0} \cdot F_0\big|_{p=1atm.} \quad (16)$$

3.2. Seed Respiration CO_2 Detection System Performance. In order to use the seed respiration CO_2 detection system to achieve real-time, high-precision, and nondestructive testing of seed respiration, we have prepared a series of test experiments to detect system performance.

When the ambient temperature changes, the laser intensity will change. In order to ensure that the detector can receive stable laser intensity during continuous seed respiration detection, we placed the seed respiration CO_2 detection system in a temperature regulator (MXA600, China) to test the detected laser intensity at different temperatures. With 5°C as the step size, set the temperature variable in the range of 5°C–45°C, and a temperature current controller is used to control the output of the 2004 nm DFB laser. Under the condition of constant laser source output, test the laser intensity change for 1 hour continuously. A photodetector is used to convert the optical signal into an electrical signal, and the voltage amplitude is used to express the laser intensity. The test voltage output is shown in Figure 9 with a fluctuation of about 1.7%, which means that the output laser intensity of the double-layer seed respiration device fluctuates very little without interference. It can be seen that the seed respiration CO_2 detection system has good laser output stability and can meet the requirements of seed respiration measurement.

In order to analyze the linearity of the seed respiration CO_2 detection system, we prepared different concentrations of standard CO_2 for testing under the conditions of 20°C and 1 atm. Before the testing, pour high-purity nitrogen into the Herriott cell for 5-6 minutes to drain the gas in the container and keep the modulation and demodulation parameters unchanged during the measurement. The second harmonic absorption signal of CO_2 is calculated according to the EMD-SG algorithm and the PSD algorithm as shown in Figure 10(a). The peak value of the 2*f* signal and the CO_2 concentration present a good linear relationship as shown in Figure 10(b) (adj. $R^2 \approx 0.999$), indicating that the EMD-SG, PSD algorithm, and modulation and demodulation parameters used in this article are suitable for CO_2 detection in this system.

In order to further analyze the stability of the system, Allan variance is introduced. Allan variance is not only an important indicator of the stability of the detection system but also can predict the detection limit. We flush in 3008 ppm CO_2 standard gas into the Herriott cell and calculated the Allan variance during the 1000 s. It can be seen from Figure 11 that the Allan variance shows a trend of decreasing first and then increases with the integration time. When the integration time is 1/7 s, the Allan variance is 143.34 ppm. As the integration time increases, the stability of the system is better, and the Allan variance decreases. When the integration time is equal to 51 s, the detection limit of the system is 1.23 ppm. This is because increasing the integration time can reduce Gaussian noise effectively, thereby reducing the detection limit and improving system stability. Then, mainly due to the influence of system drift and noise, Allan variance begins to increase again.

The repeatability of the seed respiration CO_2 detection system can be calculated based on the relative standard deviation (RSD). In the same measurement environment as possible, 1008 ppm of standard CO_2 is flushed into the double-layer seed respiration device and sealed, and repeated measurements are performed 50 times from time to time. The RSD of our developed system is calculated to be 0.00046. Table 1 compares the seed respiration CO_2 detection system with commonly used CO_2 detection methods. Compared with the widely used NDIR CO_2 sensor and gas chromatography, the seed respiration CO_2 detection system has better repeatability, and the detection limit is basically the same as gas chromatography, which is much higher than that of the NDIR CO_2 sensor. When the measuring frequency is about 0.2 Hz, the overall performance of the seed respiration CO_2 detection system is better. In addition, compared with the gas chromatography, the seed respiration CO_2 detection system has the advantages of simple operation, no need for assistance such as carrier gas, no sampling limitation, and direct concentration inversion.

In order to compare the stability of the seed respiration CO_2 detection system and the NDIR CO_2 sensor during continuous measurement, we used the above two detection methods to measure 702 ppm standard CO_2 continuously for about 30 minutes. (Because the gas chromatography needs to collect gas and inject it into the device before detecting, it is not suitable for high-resolution continuous monitoring of seed respiration intensity, so the gas chromatography is not used as a comparison object.) Figure 12(a) shows two methods within 30 minutes for the detection results of 702 ppm standard CO_2. The measurement frequency of the seed respiration CO_2 detection system is

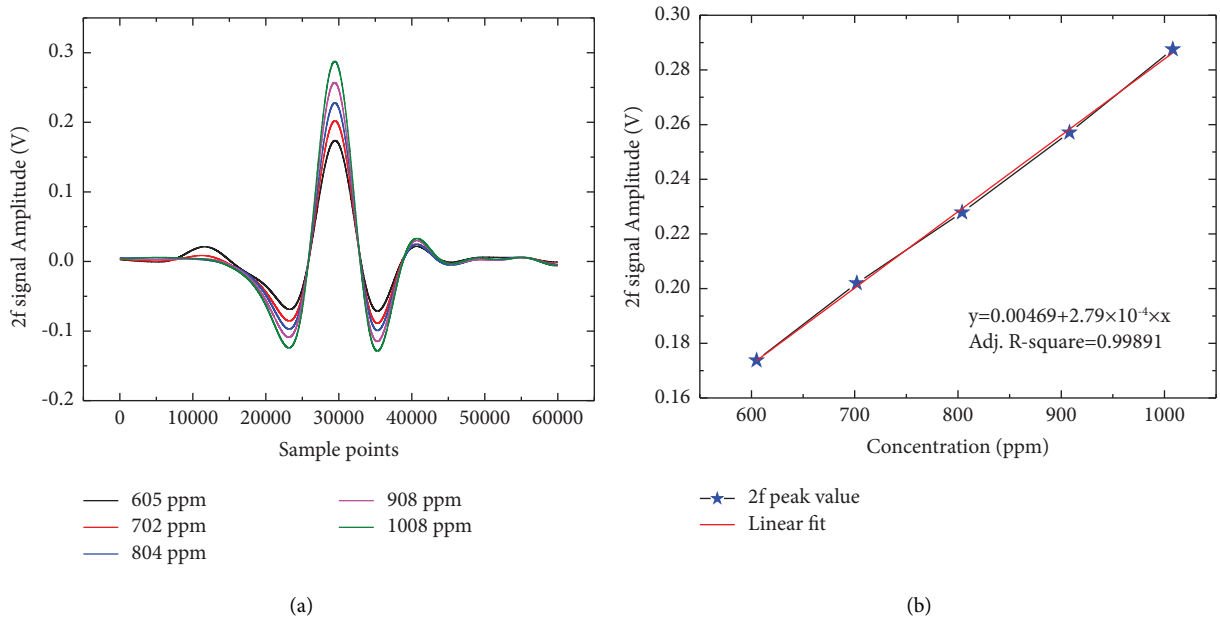

Figure 10: CO_2 calibration and linearity analysis. (a) Second harmonic signal of CO_2 at 605 ppm, 702 ppm, 804 ppm, 908 ppm, and 1008 ppm; (b) second harmonic peak fit curve of CO_2 at 605 ppm, 702 ppm, 804 ppm, 908 ppm, and 1008 ppm.

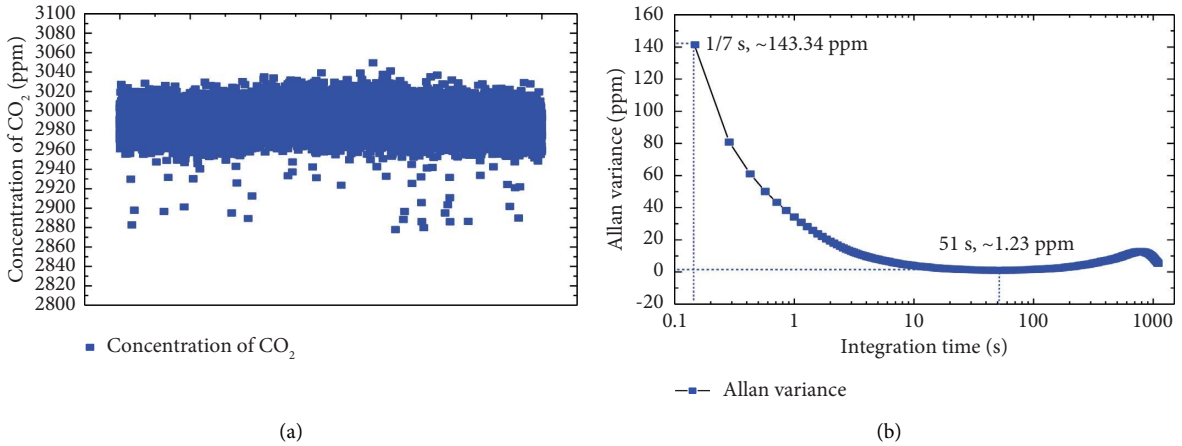

Figure 11: Allan deviation analyses of CO_2 detection limit. (a) Concentration of CO_2. (b) Allan variance.

Table 1: Performance comparison between seed respiratory CO_2 detection system with two commonly used CO_2 detection methods.

	Detection limit	RSD	Typical measurement frequency	Reference
NDIR CO_2 sensor	30 ppm–50 ppm	0.03	0.1 Hz	[33, 34]
Gas chromatography	0.8 ppm–1.5 ppm	<1.5	About 0.001 Hz	[35, 36]
Seed respiratory CO_2 detection system[a]	1.23 ppm	0.00046	About 0.2 Hz	

[a]This work.

significantly higher than that of the NDIR CO_2 sensor, with a good ability to capture the details of signal changes. During the test, both systems fluctuate within a certain range. Figures 12(b) and 12(c) calculate the residuals of the 702 ppm standard gas measured by the two methods, respectively. The fluctuation range of the seed respiration CO_2 detection system is about 5 ppm–7 ppm and the fluctuation range of the NDIR CO_2 sensor is about 20 ppm–28 ppm. Obviously, the measurement results of our developed system are more stable, and the fluctuation range is much lower than that of the NDIR CO_2 sensor. Therefore, the seed respiration CO_2 detection system is much more suitable for

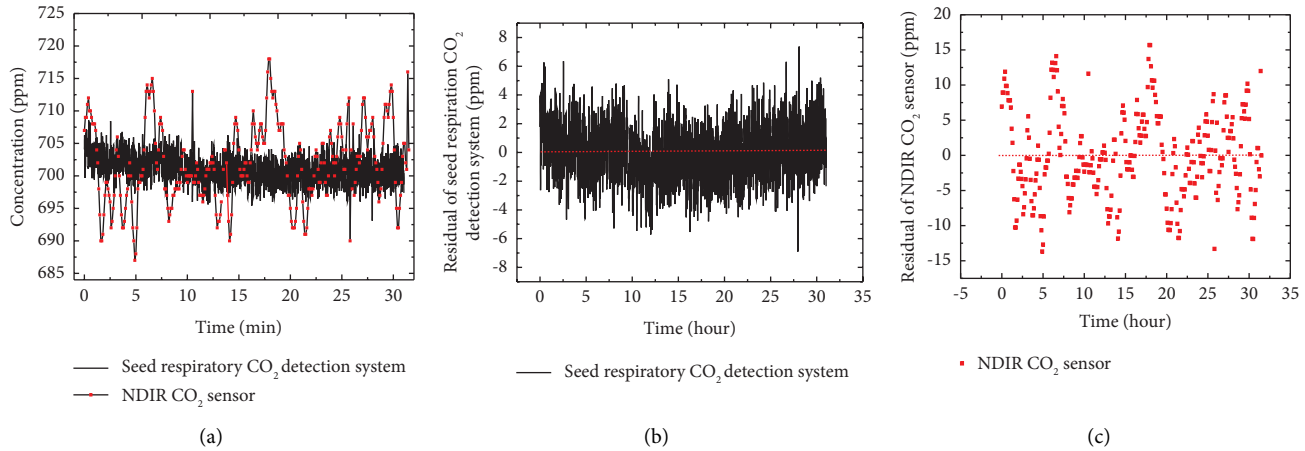

Figure 12: Stability test of the seed respiration CO_2 detection system and the NDIR CO_2 sensor. (a) Test results of 702 ppm CO_2 detection with the seed respiration CO_2 detection system and NDIR CO_2 sensor; (b) residual of the seed respiration CO_2 detection system at 702 ppm; (c) residual of NDIR CO_2 sensor at 702 ppm.

Table 2: Seed respiration CO_2 detection system measures the respiration intensity and respiration rate of 1 g sweet corn seeds and waxy corn seeds.

Time (hour)	Sweet corn seeds respiratory intensity (ppm)	Sweet corn seeds respiratory rate (ppm/h))	Waxy corn seeds respiratory intensity (ppm)	Waxy corn seeds respiratory rate (ppm/h))
0.5	128.8	257.6	15.3	30.6
1.0	333.7	409.7	39.1	47.6
1.5	587.9	508.6	73.1	68.1
2.0	886.6	597.2	115.4	84.6
2.5	1153.5	533.9	160.4	90.1
3.0	1465.7	624.3	207.9	95.1
3.5	1770.3	609.1	255.4	94.8
4.0	2059.1	577.6	301.1	91.4
4.5	2317.1	516.1	347.9	93.6
5.0	2546.5	458.7	392.8	89.9
5.5	2732.9	373.1	436.6	87.6
6.0	2918.2	370.1	478.5	83.7

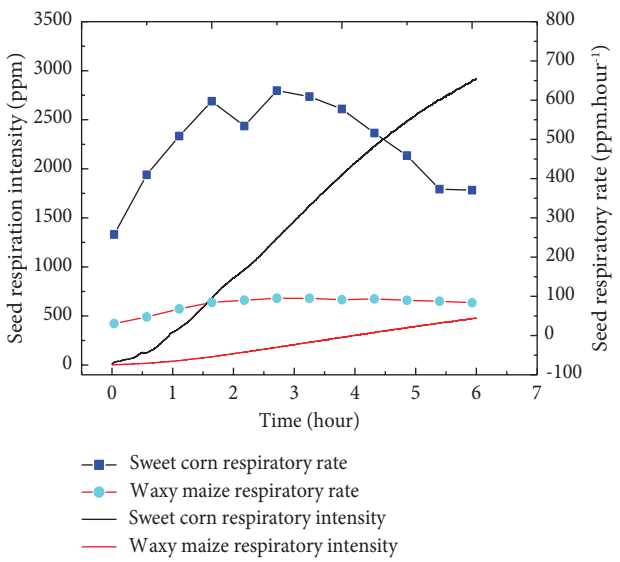

Figure 13: Variation trend of respiration intensity and respiration rate of 1 g sweet corn seeds and waxy corn seeds.

detecting the respiratory intensity of a small amount of seeds.

In order to verify that our developed system can detect the CO_2 concentration produced by seed respiration in real time and with high accuracy, we selected a small amount of sweet corn seeds and waxy corn seeds (1 g, about 40 seeds) as samples to measure the respiration intensity in a laboratory environment and calculate breathing rate. For ensuring the accuracy of the seed respiration rate calculation and taking the amount of calculation into account, we calculated the seed respiration rate every 0.5 hours. The average value of 20 sampling points before and after each time interval was taken as the seed respiration intensity at that moment shown in Table 2.

Figure 13 shows the changes in the intensity and respiration rate of less corn seeds (1 g) visually and carefully. We can find that with time increasing, the respiration intensity of sweet corn seeds and waxy corn seeds gradually increases. The respiration intensity and respiration rate changes of sweet corn seeds and waxy corn seeds in the same weight are different. The respiration intensity of sweet corn

seeds changes faster, and the respiration rate changes of waxy corn seeds are more uniform. The experiments also show that the seed respiration CO_2 detection system can achieve high-resolution continuous observation of a small amount of seed respiration and show detailed information such as the change trend of seed respiration intensity and the details of respiration rate changes. Using this system to measure the respiration intensity and respiration rate of different varieties of seeds to observe their respiration process, we can summarize and analyze the respiration changes of different varieties seeds and further study physiological and biochemical issues such as seed vigor.

4. Conclusions

In this study, a sensor system of a double-layer seed respiration device based on Herriott cell is designed independently and creatively, which solves the problem of unable to detect seed respiration with high precision in real time. The sensor has a volume of about 1.5 L and an effective optical path of about 21 meters. Using a 2004 nm laser as the light source, a set of the seed respiration CO_2 detection system based on WMS-TDLAS technology was built. The theoretical calculation of this system was done under different temperatures and pressures, and the concentration inversion correction equation was obtained when the temperature and pressure changed. The laser output has good stability and voltage fluctuation range is about 1.7%. The system linearity can reach about 0.999, and the detection limit is 1.23 ppm at 51 s. Compared with the commonly used NDIR CO_2 sensor and gas chromatography, our system has higher measurement frequency, lower detection limit, and better stability. Finally, we used the developed system to test the sweet corn seeds and waxy corn seeds respiration intensity of a small amount (1 g) and calculated their respiration rate. The test results showed that our system can show detailed information clearly, such as the change trend of seed respiration intensity and respiration rate. The seed respiration CO_2 detection system realizes high-precision continuous online monitoring of seed respiration and has broad application prospects in the fields of seed respiration detection and rapid nondestructive detection of seed vigor.

Data Availability

The data used to support the findings of this study are available from the corresponding authors upon request.

Conflicts of Interest

The authors declare that there are no conflicts of interest.

Authors' Contributions

L. J., Y. Z., G. Z., and Q. N. proposed the idea. L. G. and L. J. developed the seed respiration CO_2 detection system and completed the test experiments and deployment in the laboratory. L. G., Y. Z., and Q. L. performed the data process. L. G., Y. Z., and Q. T. wrote the draft of the manuscript. All authors have read and agreed to the published version of the manuscript. Lu Gao and Ying Zang contributed equally to this work.

Acknowledgments

This research was funded by General Scientific Research Projects of Education of Zhejiang Province Projects (Y201941626), Huzhou Public Welfare Applied Research Project (2021GZ30 and 2021GZ23), and the National Natural Science Foundation of China (31701512).

References

[1] M. A. Horbach, J. A. L. Dranski, U. C. Malavasi, and M. d. M. Malavasi, "Physiological quality and seed respiration of primed Jatropha curcas seeds," *Acta Botanica Brasilica*, vol. 32, no. 1, pp. 63–69, 2017.

[2] Z. R. Yang, F. Guo, and D. Zhang, "Changes of germination and respiration physiology of Allium mongolicum seeds under different storage times," *(Journal of Northwest A&F University Nat. Sci. Ed.)*, vol. 49, no. 11, pp. 92–114, 2021.

[3] L. Gorim and F. Asch, "Seed coating reduces respiration losses and affects sugar metabolism during germination and early seedling growth in cereals," *Functional Plant Biology*, vol. 42, no. 2, pp. 209–218, 2015.

[4] H. X. Li, J. W. Xu, and M. L. Cai, "Improved method for measuring respiratory rate of plant seeds using small-skap-method," *Chinese Journal of Biology*, vol. 32, no. 183, pp. 100–102+106, 2015.

[5] Y. W. Wang, J. J. Yuan, and M. Q. Ma, "The effect of illumination on the Germination process of Black soybean seed," *Seeds*, vol. 36, no. 290, pp. 99–102, 2017.

[6] N. F. Chen, G. W. Zhao, and T. L. Zhong, "Application of oxygen sensing technology in seed vigor testing of Castanea mollissima," *Journal of Fruit Science*, vol. 35, no. 1, pp. 74–81, 2018.

[7] T. L. Zhong and G. W. Zhao, "Application of oxygen-sensing technology to measure seed quality of Ginkgo biloba," *Journal of Forestry Research*, vol. 28, no. 4, pp. 725–731, 2017.

[8] C. Patanè and G. Avola, "A seed respiration-based index of cold-sensitivity during imbibition in four macrothermal species," *Acta Physiologiae Plantarum*, vol. 35, no. 3, pp. 911–918, 2013.

[9] 李. Li Xiang-xian, 徐. Xu Liang, 高. Gao Min-guang, 童. Tong Jing-jing, and 刘. Liu Jian-guo, "Fourier transform infrared greenhouse analyzer for gases and carbon isotope- ratio," *Optics and Precision Engineering*, vol. 22, no. 9, pp. 2359–2368, 2014.

[10] Y. X. Meng, T. G. Liu, K. Liu et al., "A modified empirical mode decomposition algorithm in TDLAS for gas detection," *IEEE Photonics Journal*, vol. 6, no. 6, pp. 1–7, 2014.

[11] C. Liu, Z. Cao, Y. Lin, L. Xu, and H. McCann, "Online cross-sectional monitoring of a swirling flame using TDLAS tomography," *IEEE Transactions on Instrumentation and Measurement*, vol. 67, no. 6, pp. 1338–1348, 2018.

[12] X. R. Zhu, S. C. Yao, W. Ren, Z. M. Lu, and Z. H. Li, "TDLAS monitoring of carbon dioxide with temperature compensation in power plant exhausts," *Applied Sciences*, vol. 9, no. 3, pp. 442–176, 2019.

[13] O. Witzel, A. Klein, C. Meffert, C. Schulz, S. A. Kaiser, and V. Ebert, "Calibration-free, high-speed, in-cylinder laser absorption sensor for cycle-resolved, absolute H_2O measurements in a production IC engine," *Proceedings of the Combustion Institute*, vol. 35, no. 3, pp. 3653–3661, 2015.

[14] R. Ghorbani and F. M. Schmidt, "ICL-based TDLAS sensor for real-time breath gas analysis of carbon monoxide isotopes," *Optics Express*, vol. 25, no. 11, pp. 12743–12752, 2017.

[15] A. Hartmann, R. Strzoda, R. Schrobenhauser, and R. Weigel, "CO_2 sensor for mainstream capnography based on TDLAS," *Applied Physics B: Photophysics and Laser Chemistry*, vol. 116, no. 4, pp. 1023–1026, 2014.

[16] Z. Liu, C. Zheng, T. Zhang et al., "Midinfrared sensor system based on tunable laser absorption spectroscopy for dissolved carbon dioxide analysis in the south China sea: system-level integrationand deployment," *Analytical Chemistry*, vol. 92, no. 12, pp. 8178–8185, 2020.

[17] L. Lan, H. Ghasemifard, Y. Yuan et al., "Assessment of urban CO2 measurement and source attribution in munich based on TDLAS-WMS and trajectory analysis," *Atmosphere*, vol. 11, no. 1, pp. 58–69, 2020.

[18] Z. Zhang, M. Li, J. Guo, B. Du, and R. Zheng, "A portable tunable diode laser absorption spectroscopy system for dissolved CO_2 detection using a high-efficiency headspace equilibrator," *Sensors*, vol. 21, no. 5, p. 1723, 2021.

[19] F. Xin, J. Li, J. Guo et al., "Measurement of atmospheric CO_2 column concentrations based on open-path TDLAS," *Sensors*, vol. 21, no. 5, p. 1722, 2021.

[20] Q. X. He, P. P. Dang, Z. W. Liu, C. T. Zheng, and Y. D. Wang, "TDLAS–WMS based near-infrared methane sensor system using hollow-core photonic crystal fiber as gas-chamber," *Optical and Quantum Electronics*, vol. 49, no. 3, pp. 115–211, 2017.

[21] A. Huang, Z. Cao, W. Zhao, H. Zhang, and L. Xu, "Frequency-division multiplexing and main peak scanning WMS method for TDLAS tomography in flame monitoring," *IEEE Transactions on Instrumentation and Measurement*, vol. 69, no. 11, pp. 9087–9096, 2020.

[22] G. B. Rieker, J. B. Jeffries, and R. K. Hanson, "Calibration-free wavelength-modulation spectroscopy for measurements of gas temperature and concentration in harsh environments," *Applied Optics*, vol. 48, no. 29, p. 5546, 2009.

[23] A. Seidel, S. Wagner, A. Dreizler, and V. Ebert, "Robust, spatially scanning, open-path TDLAS hygrometer using retro-reflective f-oils for fast tomographic 2-D water vapor concentration field measurements," *Atmospheric Measurement Techniques*, vol. 8, no. 5, pp. 2061–2068, 2015.

[24] M. E. Webber, R. Claps, F. V. Englich, F. K. Tittel, J. B. Jeffries, and R. K. Hanson, "Measurements of NH_3 and CO_2 with distributed feedback diode lasers near 2.0 μm in bioreactor vent gases," *Applied Optics*, vol. 40, no. 24, pp. 4395–4403, 2001.

[25] J. B. McManus, M. S. Zahniser, D. D. Nelson et al., "Recent progress in laser-based trace gas instruments: performance and noise analysis," *Applied Physics B: Photophysics and Laser Chemistry*, vol. 119, no. 1, pp. 203–218, 2015.

[26] G. Zhao, W. Tan, M. Jia et al., "Intensity stabilized fast-scanned direct absorption spectroscopy instrumentation based on a distributed feedback laser with detection sensitivity down to 4×10^{-6}," *Sensors*, vol. 16, no. 9, p. 1544, 2016.

[27] P. Zhimin, D. Yanjun, J. Junwei, L. Lijuan, D. Yanjun, and L. Zheng, "First harmonic with wavelength modulation spectroscopy to measure integrated absorbance under low absorption," *Optics Express*, vol. 21, no. 20, pp. 23724–23735, 2013.

[28] L. J. Lan, Y. J. Ding, Z. M. Peng, Y. J. Du, Y. F. Liu, and Z. Li, "Multi-harmonic measurements of line shape under low absorption conditions," *Applied Physics B: Photophysics and Laser Chemistry*, vol. 117, no. 2, pp. 543–547, 2014.

[29] L. S. Rothman, C. P. Rinsland, A. Goldman et al., "The HITRAN molecular spectroscopic database and HAWKS (HITRAN atmospheric workstation): 1996 edition," *Journal of Quantitative Spectroscopy and Radiative Transfer*, vol. 60, no. 5, pp. 665–710, 1998.

[30] T. Borsdorff, J. aan de Brugh, A. Schneider et al., "Improving the TROPOMI CO data product: update of the spectroscopic database and destriping of single orbits," *Atmospheric Measurement Techniques*, vol. 12, no. 10, pp. 5443–5455, 2019.

[31] P. Liu, W. Z. Huang, W. T. Zhang, and F. Li, "An EMD-SG algorithm for spectral noise reduction of FBG-FP static strain sensor," *IEEE Photonics Technology Letters*, vol. 29, no. 10, pp. 814–817, 2017.

[32] J. S. Li, H. Deng, P. F. Li, and B. L. Yu, "Real-time infrared gas detection based on an adaptive Savitzky–Golay algorithm," *Applied Physics B: Photophysics and Laser Chemistry*, vol. 120, no. 2, pp. 207–216, 2015.

[33] C. B. Yang, K. D. Romanak, R. C. Reedy, S. D. Hovorka, and R. H. Trevino, "Soil gas dynamics monitoring at a CO_2-EOR site for leakage detection," *Geomechanics and Geophysics for Geo-Energy and Geo-Resources*, vol. 3, no. 3, pp. 351–364, 2017.

[34] J. Kaur, V. Adamchuk, J. Whalen, and A. A. Ismail, "Development of an NDIR CO_2 sensor-based system for assessing soil toxicity using substrate-induced respiration," *Sensors*, vol. 15, no. 3, pp. 4734–4748, 2015.

[35] V. M. Vorotyntsev, G. M. Mochalov, and I. V. Baranova, "Gas chromatographic determination of admixtures of permanent gases, CO, CO_2, and hydrocarbons in methylsilane," *Journal of Analytical Chemistry*, vol. 68, no. 2, pp. 152–155, 2013.

[36] F. J. Santos and M. T. Galceran, "The application of gas chromatography to environmental analysis," *TrAC, Trends in Analytical Chemistry*, vol. 21, no. 9-10, pp. 672–685, 2002.